Conservative Scheme for Numerical Modeling of Flow in Natural Geometry

Michele Catella[1]; Enio Paris[2]; and Luca Solari[3]

Abstract: A numerical model is proposed to compute one-dimensional open channel flows in natural streams involving steep, nonrectangular, and nonprismatic channels and including subcritical, supercritical, and transcritical flows. The Saint-Venant equations, written in a conservative form, are solved by employing a predictor-corrector finite volume method. A recently proposed reformulation of the source terms related to the channel topography allows the mass and momentum fluxes to be precisely balanced. Conceptually and algorithmically simple, the present model requires neither the solution of the Riemann problem at each cell interface nor any special additional correction to capture discontinuities in the solution such as artificial viscosity or shock-capturing techniques. The resulting scheme has been extensively tested under steady and unsteady flow conditions by reproducing various open channel geometries, both ideal and real, with nonuniform grids and without any interpolation of topographic survey data. The proposed model provides a versatile, stable, and robust tool for simulating transcritical sections and conserving mass.

DOI: 10.1061/(ASCE)0733-9429(2008)134:6(736)

CE Database subject headings: Open channels; Unsteady flow; Numerical models; Geometry; Channel flow; Wave propagation; Two-dimensional models.

Introduction

The prediction of flood wave propagation in a natural channel is an important feature in hydraulic engineering analysis and design for river management and civil protection. Apart from classical one-dimensional schemes, two-dimensional (2D) models have extensively evolved and papers on three-dimensional models are increasing in the scientific literature. However 2D schemes are commonly restricted to the analysis of a particular limited reach region due to the computational cost and the requirement of detailed topographic information, while 3D modeling is mainly employed in the case of schematic geometries. For many practical applications and particularly for the prediction of discharge and water level profiles of unsteady flows along river systems, the Saint-Venant equations still remain the main tool. Therefore, numerical schemes of shallow water flows have significantly developed in recent years.

Numerical schemes developed to solve the Saint-Venant equations are mainly based on finite-difference or finite-volume schemes. Several numerical techniques are employed, such as the modified Godunov method (Savic and Holly 1993), the HLL approximate Riemann solver (Mingham and Causon 1998; Sanders 2001), the total variation diminishing (TVD) schemes (Garcia-Navarro et al. 1992; Wang et al. 2000; Burguete and Garcia-Navarro 2001), the flux vector splitting method (Bermudez and Vazquez 1994; Jin and Fread 1997), the flux difference splitting method (Alcrudo et al. 1992), the essentially nonoscillatory (ENO) scheme (Nujić 1995), the Petrov–Galerkin finite-element scheme (Yang et al. 1993), the space-time conservation method (Molls and Molls 1998), and the second-order TVD combined with second-order ENO scheme (Tseng et al. 2001).

Notwithstanding the various schemes proposed, numerous difficulties still arise in the computation of unsteady conditions in irregular and steep channels with transcritical flows or discontinuities (Wang et al. 2000; Capart et al. 2003; Ying et al. 2004).

In the present paper a numerical scheme capable of dealing with shocks and various types of steady and unsteady flow transition in nonrectangular and nonprismatic channels and assuring the mass conservation and the momentum balance is achieved. In nonprismatic channels with irregular geometry and steep slope, particular attention must be directed to the treatment of the source terms (Garcia-Navarro and Vázquez-Cendón 2000; Burguete and Garcia-Navarro 2001; Zhou et al. 2001; Ying et al. 2004). The exact balance of the hydrostatic pressure due to the channel geometry variations at every intercell node of the spatial discretization is achieved by a reformulation of the Saint-Venant equations as shown by Schippa and Valiani (2002) and Capart et al. (2003).

In the proposed scheme the governing equations are written in a conservative form for the unknown variables flow discharge and wetted cross-sectional area. They are formulated employing an explicit finite-volume scheme over an irregular computational domain where each cell is delimited by the river cross sections which, in general, are not equidistant. The solution is obtained by means of an explicit predictor-corrector method.

The major novelties here introduced are mainly associated

[1]Ph.D. Student, Dept. of Civil and Environmental Engineering, Univ. of Florence, via S. Marta 3, 50139 Firenze, Italy. E-mail: m.catella@physis.net

[2]Professor, Dept. of Civil and Environmental Engineering, Univ. of Florence, via S. Marta 3, 50139 Firenze, Italy. E-mail: eparis@dicea.unifi.it

[3]Researcher, Dept. of Civil and Environmental Engineering, Univ. of Florence, via S. Marta 3, 50139 Firenze, Italy (corresponding author). E-mail: luca.solari@dicea.unifi.it

Note. Discussion open until November 1, 2008. Separate discussions must be submitted for individual papers. To extend the closing date by one month, a written request must be filed with the ASCE Managing Editor. The manuscript for this paper was submitted for review and possible publication on June 17, 2005; approved on August 6, 2007. This paper is part of the ***Journal of Hydraulic Engineering***, Vol. 134, No. 6, June 1, 2008. ©ASCE, ISSN 0733-9429/2008/6-736–748/$25.00.

both with the evaluation of the fluxes, which are calculated at the two interfaces delimiting each cell employing the values of the hydraulic variables obtained at the previous substep, and with the assignment of the unknown variables. In particular for the flow discharge an unconditional upwinding is proposed, while for the wetted cross section a criterion essentially based on the average Froude number calculated in two consecutive cells is employed. These novelties make the proposed scheme different from other finite-volume methods due to the fact it does not require the solution of the Riemann problem at each cell interface and it does not need any special additional correction to capture discontinuities in the solution such as artificial viscosity or shock-capturing techniques.

The proposed scheme is then tested by means of various benchmark problems. First the quiescent steady state in a rectangular channel with variable width and variable bed is simulated. A hydraulic jump in a horizontal and rectangular channel, including both constant and divergent width, and subcritical and transcritical flows with and without a shock over a bump in a frictionless flat channel with rectangular cross sections, are also reproduced under a steady condition. Finally dam break flows with dry and wet beds in a horizontal rectangular channel with no friction, partial dam break problems, and overtopping flows are modeled.

In addition, the proposed scheme is tested to reproduce the propagation of a gauged flood wave in a real natural river with steep slopes, irregular cross sections, and strong nonuniform grids including subcritical, supercritical, and transcritical flows.

Comparisons among model results, analytical solutions, experimental data, and available survey data show the model is capable of providing stable, accurate, nonoscillatory, and monotone solutions and precisely balances the mass and momentum fluxes.

Numerical Scheme

One-dimensional unsteady flows in natural channels with irregular topography can be described by the Saint-Venant equations.

A system of orthogonal Cartesian axis (x,y,z) with unit vectors $(\bar{i},\bar{j},\bar{k})$ is introduced (Fig. 1). The vertical z axis is positive upwards and the horizontal x axis, corresponding to the projection of the thalweg line on the plan $z=0$, is positive downstream. Considering small values of bottom slope, channel cross sections are assumed to be orthogonal to the x axis. As usual in the one-dimensional scheme the flow is straight in the plan.

The control volume V at the jth cell is defined by the channel reach included between two vertical cross sections $j-1/2$ and $j+1/2$ separated by a distance Δx_j. The cross sections are in general not equidistant, therefore each cell is characterized by different lengths. The wetted control surface S consists, respectively, of the upstream cross section $S_{j-1/2}$, the downstream cross section $S_{j+1/2}$, the bottom wetted surface S_l, and the water free surface S_{pl}.

The momentum equation applied to the control volume V, reads

$$\int_V \rho(-g\bar{k})dV + \int_S (-p\bar{n}+\bar{\tau})dS = \int_V \frac{\partial \rho \bar{v}}{\partial t}dV + \int_S \rho\bar{v}(\bar{v}\cdot\bar{n})dS \quad (1)$$

where ρ=density of water; g=gravitational acceleration; p=pressure; $\bar{\tau}$=shear stress (viscous+turbulent), $\bar{v}$=local velocity averaged over turbulence; and $\bar{n}$=unit vector normal to the wetted control surface and positive in the outward direction.

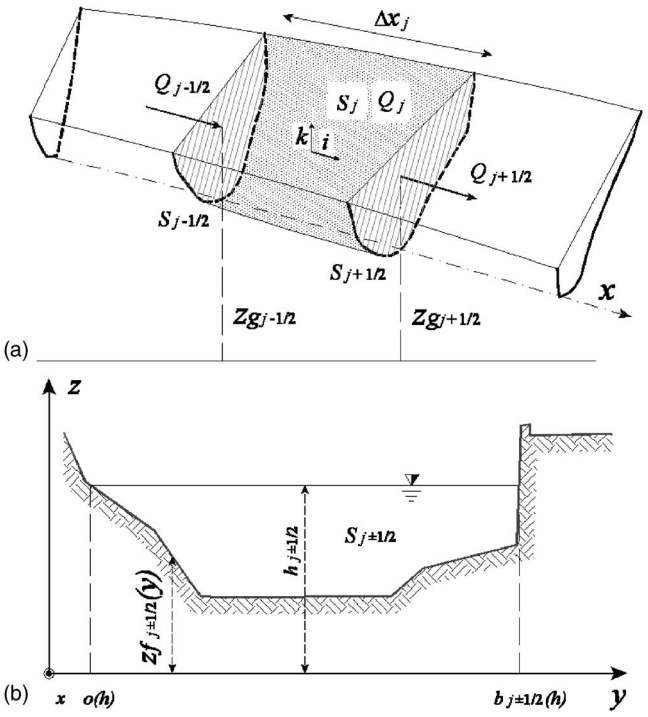

Fig. 1. (a) Definition sketch of control volume; (b) definition sketch of wetted cross section

Projecting Eq. (1) on the horizontal x axis and assuming impermeable banks, it is found that

$$\rho\frac{\partial}{\partial t}\int_{x_{j-1/2}}^{x_{j+1/2}} Q\,dx + F_{j+1/2} - F_{j-1/2} + \int_{S_l}(p\bar{n}-\bar{\tau})\cdot\bar{i}\,dS_l = 0 \quad (2)$$

where Q=liquid discharge; and $F_{j\pm1/2}$=momentum function defined as follows (see Eq. (3) and (19), Chow 1959)

$$F_{j\pm1/2} = \int_{S_{j\pm1/2}} (p+\rho v^2)\bar{i}\,dS \quad (3)$$

Particular attention is paid to the treatment of the source terms in Eq. (2) which are related both to the hydrostatic pressure and to the shear stress acting on the wetted surface S_l.

Considering two vertical cross sections separated by an infinitesimal distance dx, it is reasonable to assume that the hydrostatic pressure force in the direction of the main stream, due to the reaction of the channel walls in the case of variations in shape along this direction, can be expressed as the variation of the first moment I_1 of the wetted cross section with respect to a constrained free surface elevation h_m, as shown by Schippa and Valiani (2002) and Capart et al. (2003), and it reads

$$p\bar{n}\cdot\bar{i}\,dS_l = \gamma\left.\frac{\partial I_1}{\partial x}\right|_{h_m} dx = \gamma\left.\frac{\partial S\cdot(h-z_g)}{\partial x}\right|_{h_m} dx$$
$$= \gamma\cdot\left(\frac{\partial S}{\partial x}(h_m - z_g) - S\frac{\partial z_g}{\partial x}\right)dx \quad (4)$$

where γ=unit weight; h_m=average elevation of the water surface within the cell; and z_g=center mass elevation of the wetted cross

section. Integrating Eq. (4) over the jth cell and assuming a linear variation of all the variables (water surface elevation, wetted cross-sectional area, and center mass elevation) the following expression is obtained

$$\int_{S_l} p\bar{n}\cdot\bar{i}\,dS_l = \gamma\cdot[S_{j+1/2}(h_{mj}-z_{gj+1/2}) - S_{j-1/2}(h_{mj}-z_{gj-1/2})] \quad (5)$$

The derivation of Eq. (5) is given in the Appendix.

As a first approximation the shear stress acting on the wetted surface S_l is evaluated in each cell as the average of the shear forces per unit length acting on the two interfaces delimiting the cell

$$\int_{S_l} \bar{\tau}\cdot\bar{i}\,dS_l = \rho\frac{\Delta x_j}{2}\left[B_{j+1/2}\left(\frac{Q|Q|}{(CS)^2}\right)_{j+1/2} + B_{j-1/2}\left(\frac{Q|Q|}{(CS)^2}\right)_{j-1/2}\right] \quad (6)$$

where $B_{j\pm1/2}$=wetted perimeter; and C=dimensionless Chézy coefficient defined as the ratio between the dimensional Chézy coefficient (see Eq. 5-2, Chow 1959) and $\sqrt{g}$.

Substituting Eqs. (5) and (6) into Eq. (2) the momentum equation reads

$$\frac{\partial}{\partial t}\int_{x_{j-1/2}}^{x_{j+1/2}} Q\,dx + \left[\beta\frac{Q|Q|}{S} + gI_1\right]_{x_{j-1/2}}^{x_{j+1/2}} - g[S_{j+1/2}(h_{mj}-z_{gj+1/2}) - S_{j-1/2}(h_{mj}-z_{gj-1/2})] + \frac{\Delta x_j}{2}\left[B_{j+1/2}\left(\frac{Q|Q|}{(CS)^2}\right)_{j+1/2} + B_{j-1/2}\left(\frac{Q|Q|}{(CS)^2}\right)_{j-1/2}\right] = 0 \quad (7)$$

where β=Boussinesq velocity distribution coefficient [see Eqs. (2)–(5), Chow 1959] estimated as

$$\beta = \frac{\int_0^{b(h)}(h-z_f(y))dy\cdot\int_0^{b(h)}(h-z_f(y))^2K_1(h,y)dy}{\left[\int_0^{b(h)}(h-z_f(y))^{3/2}[A\ln(h-z_f(y))+B-A]dy\right]^2} \quad (8)$$

with $K_1(h,y)=[A\ln(h-z_f(y))+B+A]^2-A^2$ and having assumed in each cross section that the energy loss gradient J along the y coordinate is constant and a logarithmic velocity profile applies along each vertical: $v(h,y)=u_*(h,y)\cdot[A\ln(h-z_f(y))+B]$; where b=free surface width; $z_f(y)$=bed elevation; and $u_*=\sqrt{g(h-z_f(y))J}$=friction velocity. In the present calculation A and B are assumed to be equal to 2.5 and 8.5, respectively (Graf 1998).

The integral form of the continuity equation under the assumption of no lateral inflow or outflow is

$$\frac{\partial}{\partial t}\int_{x_{j-1/2}}^{x_{j+1/2}} S\,dx + [Q]_{x_{j-1/2}}^{x_{j+1/2}} = 0 \quad (9)$$

The governing Eqs. (7) and (9) are the basic laws of mechanics applied on the jth cell.

Introducing the usual discretization

$$\frac{\partial}{\partial t}\int_{x_{j-1/2}}^{x_{j+1/2}} G\,dx \cong \frac{G_j^{n+1}-G_j^n}{\Delta t^n}\Delta x_j \quad (10)$$

(where G=arbitrary variable; G_j is defined within the cell and represents the average value of G over the jth cell, and n=time step index) we obtain a $2(N-1)$ equations system containing $2(N-1)$ variables that correspond to the S_j and Q_j average values of S and Q quantities in each $N-1$ cell defined by N grid points approximation of the entire reach length. The N grid points are generally provided by topographic surveys at discrete locations $x_{j+1/2}$ that are not equidistant.

The solution of the present equations system is conducted by applying an explicit two step predictor-corrector conservative scheme based on a finite-volume method. The proposed technique, composed of a sequence of two substeps in which the spatial derivatives are always taken in the same directions, reads

$$\mathbf{U}_j^p = \mathbf{U}_j^n - \frac{\Delta t^n}{\Delta x_j}[\mathbf{F}_{j+1/2}^n - \mathbf{F}_{j-1/2}^n] + \Delta t^n\mathbf{S}_j(\mathbf{U}^n,x) \quad (11)$$

$$\mathbf{U}_j^c = \mathbf{U}_j^n - \frac{\Delta t^n}{\Delta x_j}[\mathbf{F}_{j+1/2}^p - \mathbf{F}_{j-1/2}^p] + \Delta t^n\mathbf{S}_j(\mathbf{U}^p,x) \quad (12)$$

where the superscripts p and c=predictor and corrector steps; while $\mathbf{U}$, $\mathbf{F}$, and $\mathbf{S}$=vectors of conserved variables, fluxes, and source terms, respectively, defined as follows:

$$\mathbf{U}_j = \begin{bmatrix} S_j \\ Q_j \end{bmatrix} \quad (13a)$$

$$\mathbf{F}_{j\pm1/2} = \begin{bmatrix} Q \\ \beta\frac{Q|Q|}{S} + gI_1 \end{bmatrix}_{j\pm1/2} \quad (13b)$$

$$\mathbf{S}_j = \begin{bmatrix} 0 \\ \frac{g}{\Delta x_j}[S_{j+1/2}(h_{mj}-z_{gj+1/2}) - S_{j-1/2}(h_{mj}-z_{gj-1/2})] - \frac{1}{2}\left[B_{j+1/2}\left(\frac{Q|Q|}{(CS)^2}\right)_{j+1/2} + B_{j-1/2}\left(\frac{Q|Q|}{(CS)^2}\right)_{j-1/2}\right] \end{bmatrix} \quad (13c)$$

The solution at the new time level $n+1$ is then evaluated as an average between the two substeps

$$\mathbf{U}_j^{n+1} = 0.5\cdot(\mathbf{U}_j^p + \mathbf{U}_j^c) \quad (14)$$

In the present method the values of wetted cross-sectional area and liquid discharge over each cell are employed as conservative variables of the governing equations independently from the adopted spatial grid. The fluxes are computed at the two interfaces delimiting each cell employing the values of the hydraulic variables evaluated in the corresponding interfaces at the previous substep. The evaluation of the fluxes proposed here is one of the major novelties of the present scheme; indeed finite-volume schemes generally require the solution of the Riemann problem together with some special additional correction to capture discontinuities in the solution.

The criterion to assign the variables $S_{j+1/2}$ and $Q_{j+1/2}$ to the N

interfaces from the $2(N-1)$ values S_j and Q_j computed in each cell and the two boundary conditions requires particular attention. The proposal is simple and appears to be particularly suitable for natural river flow modeling, where wetted cross-sectional areas, due to the irregularities of channel topography, can be very different at the extreme vertical interfaces of each cell. To assign S, a criterion based on the Froude number of the average flow of the upstream and downstream cells across the assigned interface is applied in addition to an appropriate boundary condition at the upstream or downstream edge of the channel. The Froude number of the average flow of the jth cell reads

$$\mathrm{F}_j = \frac{(\alpha_{j-1/2} + \alpha_{j+1/2})(b_{j-1/2} + b_{j+1/2})Q_j^2}{4gS_j^3} \tag{15}$$

where α=Coriolis velocity distribution coefficient [see Eqs. (2)–(4), Chow 1959] estimated as follows:

$$\alpha = \frac{\left[\int_0^{b(h)} (h - z_f(y))dy\right]^2 \cdot \int_0^{b(h)} (h - z_f(y))^{5/2}\{K_2(h,y)\}dy}{\left[\int_0^{b(h)} (h - z_f(y))^{3/2}[A\ln(h - z_f(y)) + B - A]dy\right]^3} \tag{16}$$

with $K_2(h,y) = (A\ln(h - z_f(y)) + B)^3 - 3A(A\ln(h - z_f(y)) + B)^2 + 6A^2(A\ln(h - z_f(y)) + B) - 6A^3$.

In particular, if the average flows in the jth and $j+1$th cells are both subcritical, then $S_{j+1/2} = S_{j+1}$; if both are supercritical, then $S_{j+1/2} = S_j$. In the case of transcritical flows, if the average flows in the jth and $j+1$th cells are subcritical and supercritical, respectively, S at the $j+1/2$th intercell takes the critical value, whereas, i.e., supercritical and subcritical, respectively, a criterion based on the momentum function of the flow in the upstream and downstream cells across the assigned interface is applied. In particular, referring to Eq. (3), if $F_{j+1/2}(S_j, Q_j) > F_{j+1/2}(S_{j+1}, Q_j)$, then $S_{j+1/2} = S_j$; otherwise $S_{j+1/2} = S_{j+1}$. The proposed assignment criteria is a novelty of the present finite-volume scheme; the conserved variables are here defined as average values over the cell and they can be considered as representative of some points inside the cell.

With regard to the boundary conditions, the liquid discharge is always specified as the upstream boundary condition in both subcritical and supercritical flow regimes, while an appropriate hydraulic variable (e.g., normal depth, known water level) is specified as an up- or downstream boundary condition depending on both the particular analyzed hydraulic problem and the flow regime.

For the stability of the present explicit scheme, the Courant–Friederich–Lewy number N_{CFL} must satisfy the following condition

$$N_{\mathrm{CFL}} = \Delta t \cdot \frac{\max_j\left[\left|\frac{Q}{S}\right|_{j+1/2}\right] + \max_j\left[\left|\sqrt{\frac{g \cdot S}{\alpha \cdot b}}\right|_{j+1/2}\right]}{\min_j[\Delta x_j]} < 1$$

$$1 \leq j \leq N \tag{17}$$

Numerical Tests

In this section the proposed scheme is tested by solving nine different benchmark problems including both steady and unsteady flows.

In particular, the suitability of the schematization of the source terms, of the bed friction term, and of the hydrostatic pressure contributions acting on nonprismatic channel boundaries is specifically evaluated in Test 1 (water at rest in a channel with vertical sides, variable width, variable bed), Test 2 (hydraulic jump in a uniform rectangular horizontal channel), and Test 3 (hydraulic jump in a divergent rectangular horizontal channel), respectively. The capability to preserve mass along the channel has been tested under various steady flow conditions both in Test 4 for the case of a bump in a rectangular horizontal channel and in Test 5 for the case of a natural river involving nonrectangular cross sections and nonuniform grids. The ability of the model to track the singularity occurring at the leading edge of an advancing front on a wet and dry bed is verified in Tests 6 and 7 for the case of an idealized dam-break problem in a rectangular horizontal channel. Finally Tests 8 and 9 involving a partial dam-break problem, a hydraulic jump, and an overtopping flow in a channel with irregular geometry are carried out to investigate the overall model performance.

The accuracy of the present scheme is demonstrated by comparing the numerical solutions with analytical solutions or experimental measurements.

Test 1: Water at Rest

The numerical scheme's conservation property can be seriously damaged when the geometrical source terms are not correctly treated. In this case the scheme fails to reproduce the simple physical problem of the steady state of still water in a rectangular channel with bed slope and width variations leading to considerable oscillations of water levels and to non-negligible discharges (Garcia-Navarro and Vázquez-Cendón 2000; Schippa and Valiani 2002; Siviglia et al. 2002).

In this test the modeling of a quiescent steady state case in a 1,500 m long channel with vertical sides, variable width, variable bed, and no bed friction (Goutal and Maurel 1997) has been carried out. The channel bed profile and the width variations along the distance are reported in Fig. 2(a). A constant 12 m water level at rest is imposed at time $t=0$ s. The analytical solution is obviously zero discharge and constant water level everywhere. In the computation the channel is represented by 300 cells ($\Delta x=5$ m), N_{CFL} is set equal to 0.9, and the inflow condition is $Q=0$ m^3/s. The N_{CFL} values do not affect the solution.

The relative errors in water depth and discharge along the river reach are reported in Figs. 2(b and c), respectively, while the computed discharge hydrograph at a station located at $x=600$ m is displayed in Fig. 2(d). Results show a good agreement between computed and exact values demonstrating the scheme satisfies accurately mass and momentum conservation.

Further tests, not reported here, show the scheme performs well after introducing friction over the bed by computing no difference in the solutions.

Test 2: Hydraulic Jump in Rectangular Channel

A hydraulic jump is a stationary steady shock, which occurs whenever the flow changes from supercritical to a subcritical state by generating an abrupt rise of free water surface. This test high-

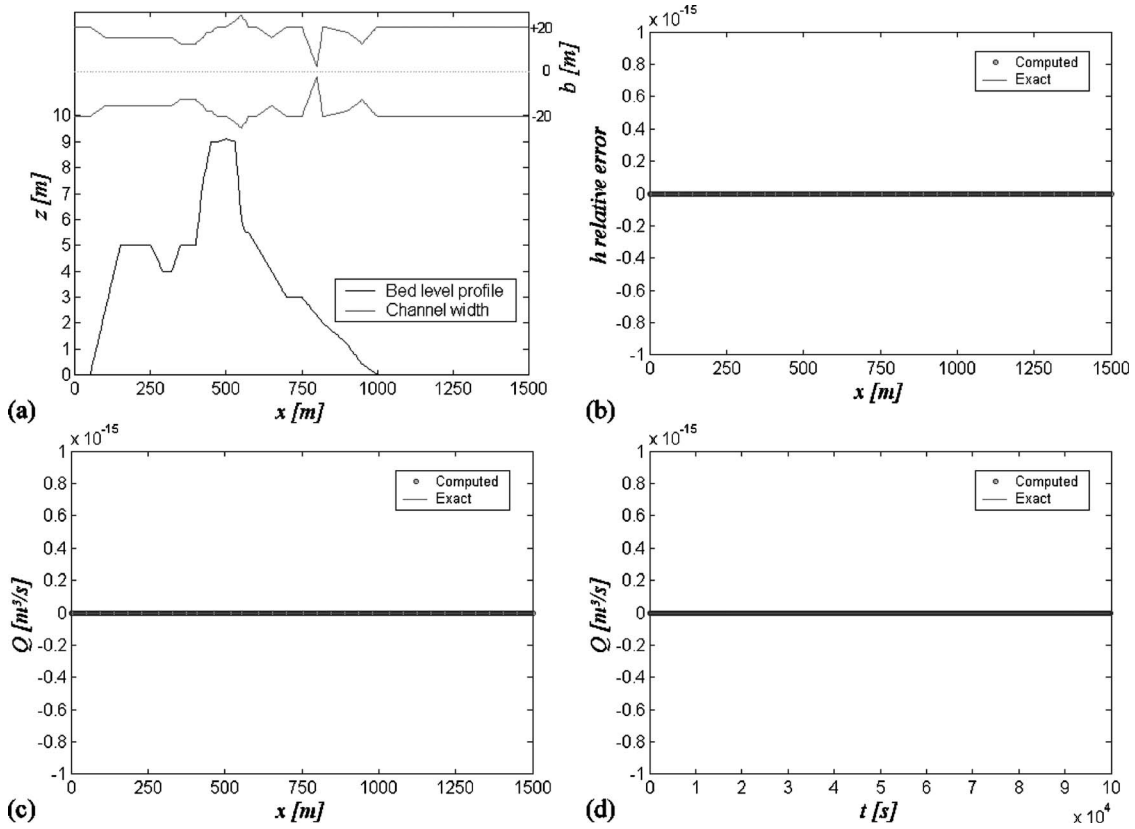

Fig. 2. Channel with vertical sides, variable width, variable bed, and no bed friction. Water at rest—no flow: (a) channel bed level and width variations; (b) water level relative error profile at steady state; (c) discharge profile at steady state; and (d) computed discharge hydrograph at station located at $x=600$ m.

lights the model's capability to accurately treat bed friction terms since the hydraulic jump location is largely determined in practice by the effect of the bed channel roughness for the case of steady boundary conditions (Zhou et al. 2001).

The numerical scheme is applied here to reproduce four different experimental runs of this hydraulic phenomenon conducted by Gharangik and Chaudhry (1991). The channel is 14 m long, 0.915 m high, and 0.46 m wide with a rectangular cross section and no bed slope. The value of the Manning coefficient is set equal to 0.014 $s/m^{1/3}$, the same value used in the numerical simulation carried out by Ying et al. (2004). In the computations the channel is represented by 50 cells ($\Delta x=0.28$ m), and N_{CFL} is set equal to 0.9. Note that the solutions are not affected by the N_{CFL} values, therefore the chosen time step size is very close to the maximum allowed by numerical stability. The flow depth and discharge at the upstream side and the flow depth at the downstream side are imposed as boundary conditions.

In run (a) of Fig. 3 the Froude number of the incoming flow is 7 and the boundary conditions are: inflow velocity 3.831 m/s, inflow water depth 0.031 m, and outflow water depth 0.265 m.

In run (b) the Froude number of the incoming flow is 6.65 and the boundary conditions are: inflow velocity 3.255 m/s, inflow water depth 0.024 m, and outflow water depth 0.195 m.

In run (c) the Froude number of the incoming flow is 5.74 and the boundary conditions are: inflow velocity 3.578 m/s, inflow water depth 0.040 m, and outflow water depth 0.286 m.

In run (d) the Froude number of the incoming flow is 2.3 and the boundary conditions are: inflow velocity 1.826 m/s, inflow water depth 0.064 m, and outflow water depth 0.168 m.

Fig. 3(a–d) show that the jump locations appear to be captured for all the runs, while the computed steady water surface profiles are in reasonable agreement with the experimental measurements especially for the runs (a–c).

Test 3: Hydraulic Jump in Divergent Channel

In Test 3, the model's ability to compute a stationary shock is determined by including the nonprismatic effects due to the channel width variations.

The numerical scheme is applied to reproduce the experimental tests conducted by Khalifa (1980) and used by Younus and Chaudhry (1994) and Capart et al. (2003) as a verification test. The horizontal channel is 2.5 m long with rectangular cross sections and the channel width along the channel is

$$b(x)=\begin{cases}0.155\ \text{m}, & x\leqslant 0.65\ \text{m}\\ 0.155+0.305/1.29\cdot(x-0.65)\ \text{m}, & 0.65\ \text{m}<x\leqslant 1.94\ \text{m}\\ 0.46\ \text{m}, & x>1.94\ \text{m}\end{cases} \tag{18}$$

In the computations the channel is represented by 50 cells ($\Delta x=0.05$ m), N_{CFL} is set equal to 0.9, and the value of the Manning coefficient is set equal to 0.020 $s/m^{1/3}$. The flow depth and discharge at the upstream side and the flow depth at the downstream side are specified as boundary conditions. The inlet flow discharge is 0.0263 m^3/s; and the upstream and downstream water depth are set equal to 0.088 and 0.195 m, respectively.

Fig. 4 shows a good agreement between computed results and experimental measurements of the steady water surface profile and the location of the hydraulic jump is also predicted well.

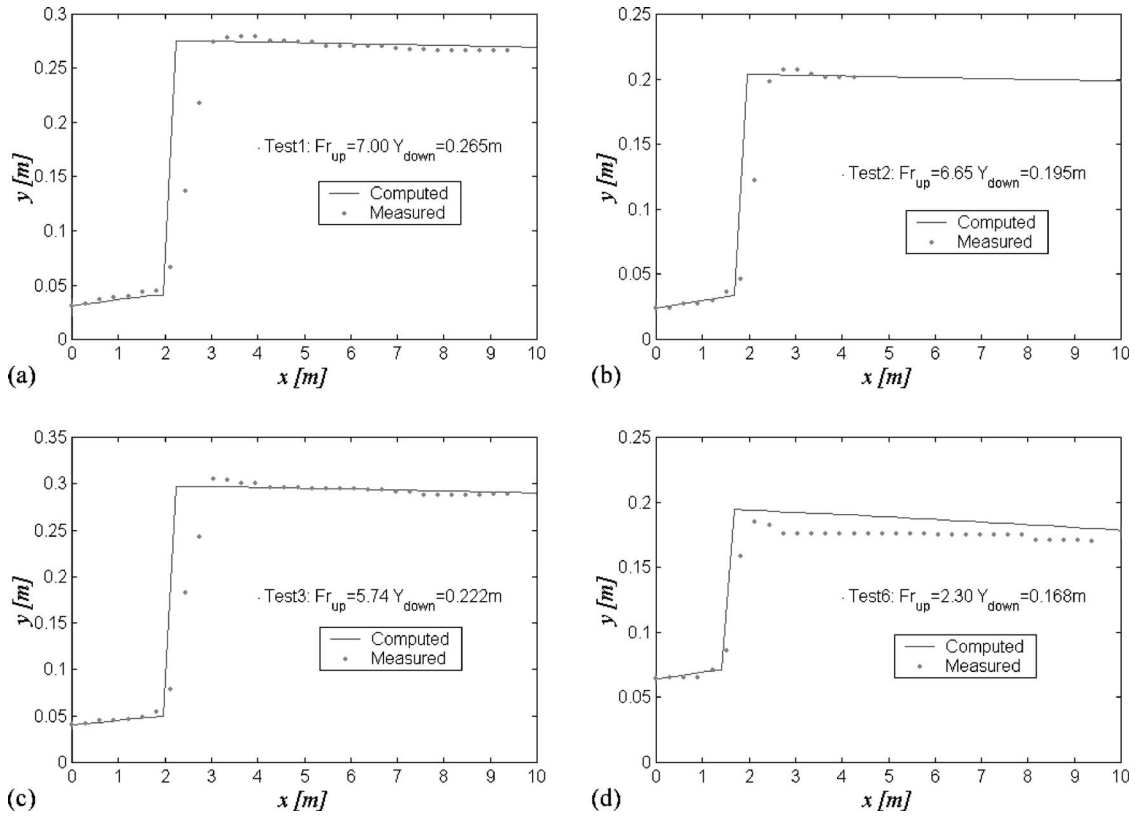

Fig. 3. Water surface profiles of four different hydraulic jumps in horizontal, rectangular channel with Manning coefficient equal to 0.014 $s/m^{1/3}$. Solid lines represent numerical results; points represent experimental data from Gharangik and Chaudhry (1991).

Test 4: Steady Flow over Bump

This is a classical test problem for subcritical and transcritical flows and is widely used to study the convergence of numerical solutions and the discharge conservation along the channel (Goutal and Maurel 1997; Vázquez-Cendón 1999; Zhou et al. 2001; Ying et al. 2004; Valiani et al. 2004).

The channel is 25 m long, and 1 m wide with rectangular cross sections and frictionless bottom topography defined by

$$z_f(x) = \begin{cases} 0 \text{ m}, & x < 8 \text{ m and } x > 12 \text{ m} \\ 0.2 - 0.05 \cdot (x - 10)^2 \text{ m}, & 8 \text{ m} \leq x \leq 12 \text{ m} \end{cases} \tag{19}$$

Depending on the initial conditions, the flow may be subcritical, transcritical with or without a steady shock, or supercritical. In the computations the channel is represented by 250 cells (Δx=0.1 m) and N_{CFL} is set equal to 0.9. Also in this test case, there is no dependence of model solutions on the N_{CFL} number.

For a transcritical flow with a shock, a discharge per unit width of q=0.18 m^2/s is imposed at the upstream boundary and h=0.33 m is specified at the downstream boundary condition. The water surface profile is plotted in Fig. 5(a), while in Figs. 5(b and c) the relative errors, respectively, of water depth and discharge along the river reach are reported. Results show that the numerical solutions of the water level and discharge are in good agreement with the analytical solutions, and the hydraulic jump location is accurately predicted.

Further tests, such as for a subcritical flow and for a transcritical flow without a shock, show an excellent agreement between numerical and analytical solutions.

In all three test cases cited above, results show that the discharge along the channel is always very satisfactorily conserved.

Test 5: Steady Flow in Natural Channel

This test case is selected to analyze the capability of the numerical scheme to preserve discharge along the channel by modeling a

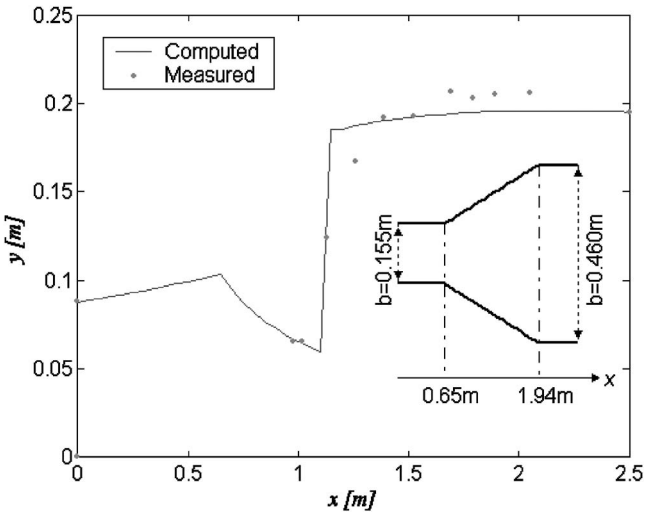

Fig. 4. Water surface profile of hydraulic jump in horizontal, rectangular, and divergent channel with Manning coefficient equal to 0.02 $s/m^{1/3}$. Solid lines represent numerical results, and points represent experimental data from Khalifa (1980). In lower-right corner channel planimetry is reported.

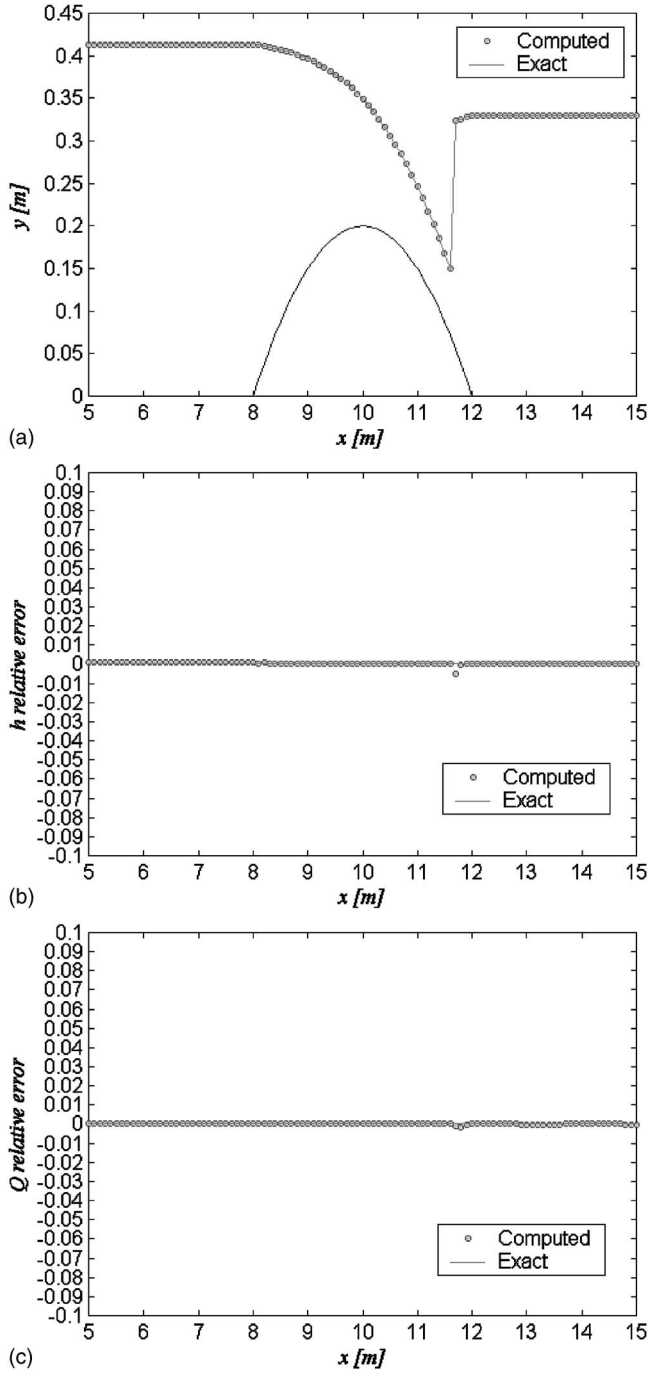

Fig. 5. Steady flow over bump in rectangular channel with flat bed and no bed friction. Subcritical to supercritical with shock: (a)–(c) water level profile; water level; and discharge relative error.

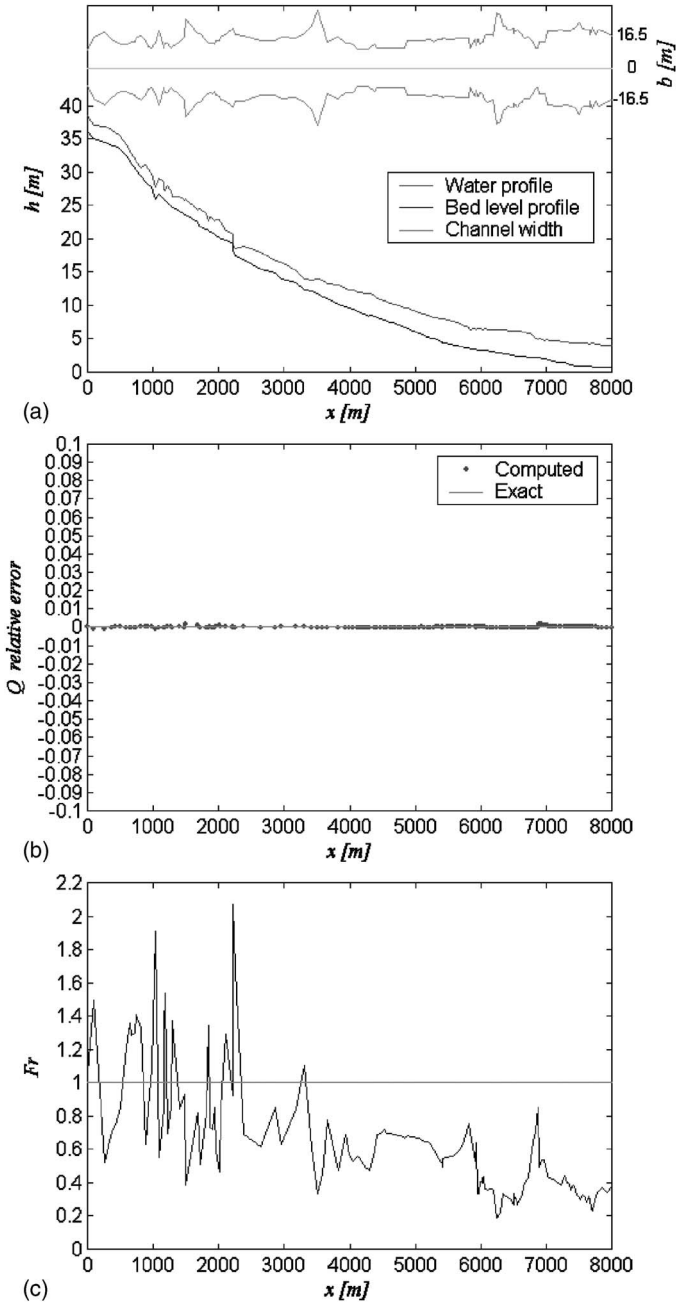

Fig. 6. Steady flow in Versilia River: (a) bed level and water surface profile and free surface river width; (b) discharge relative error; and (c) Froude number variations along distance

steady flow in a natural channel involving nonrectangular cross sections and nonuniform grids and including subcritical, supercritical, and transcritical flows.

The test case is carried out by employing the topographical data of the upper reach of about 8,000 m of the Versilia River in Tuscany, Italy. The channel reach is discretized by 169 cross sections with a strong nonuniform grid where the spatial step ranges from 2 to 264 m. In the computation, N_{CFL} is set equal to 0.9 and the Manning coefficient is set to 0.031 $s/m^{1/3}$. A uniform flow depth is specified as both upstream and downstream boundary conditions, and the discharge of the incoming flow is $Q=180$ m^3/s (2 years return period flood). Note that the model solution is not dependent on the N_{CFL} number.

The plan view of the free surface width variation along the channel, the bed level profile, and the computed water surface profile at the steady state are plotted in Fig. 6(a). Fig. 6(b) shows that the numerical scheme satisfies mass conservation precisely in this test case. Moreover the Froude number is shown as a function of channel distance in Fig. 6(c), showing that several flow transitions occur.

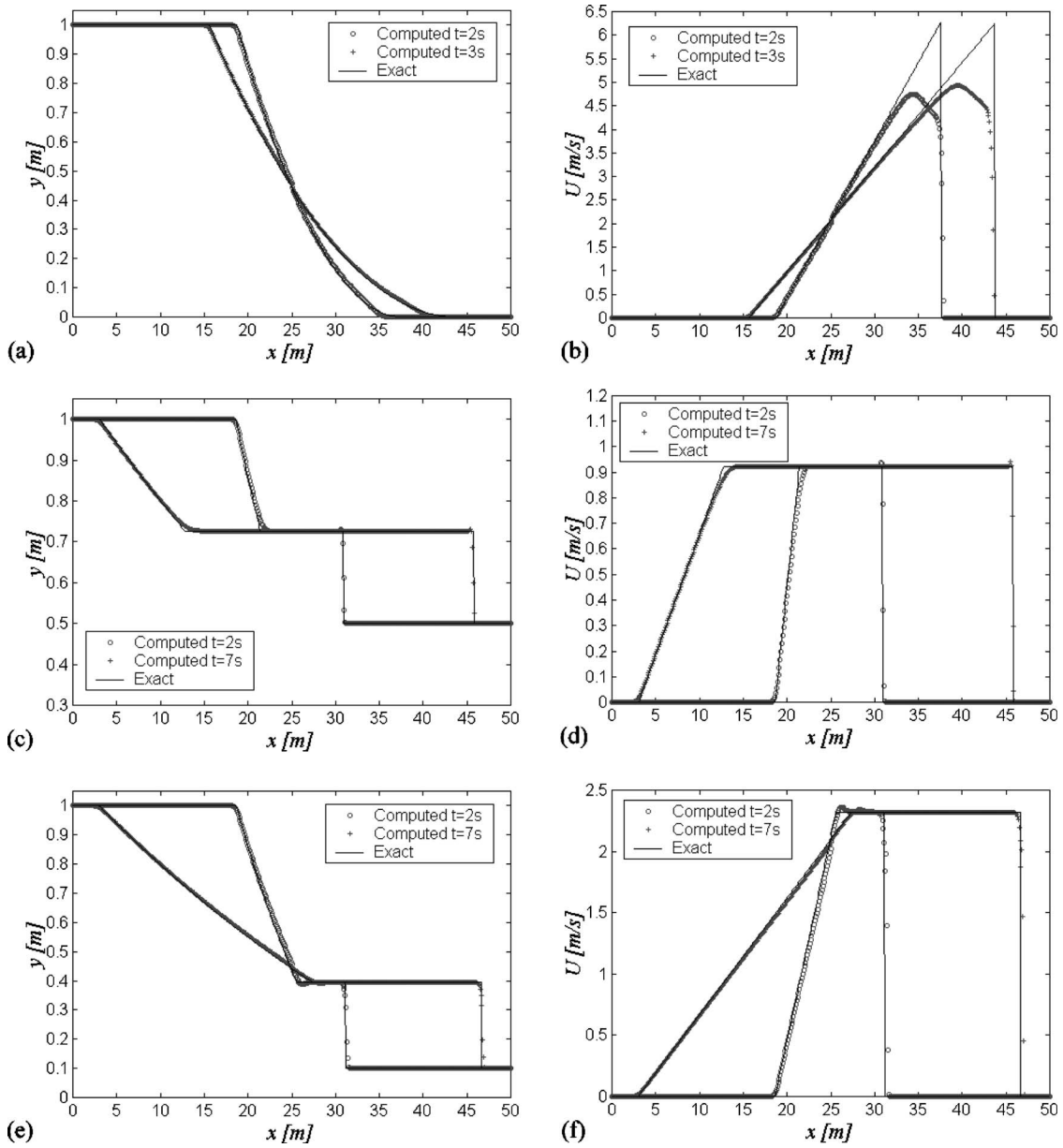

Fig. 7. Numerical solutions of dam-break problem in horizontal, rectangular channel with no bed friction. Water surface, and velocity profiles: (a)–(b) dam break with dry bed; (c)–(d) dam-break with wet bed and downstream stagnant water depth=0.5 m; (e)–(f) dam break with wet bed and downstream stagnant water depth=0.1 m.

Test 6: Idealized Dam-Break Problem with Dry Bed

The idealized dam-break problem in a rectangular channel with a dry bed is an arduous benchmark test to judge the model's performance with the singularity that occurs at the leading edge of the advancing front.

The channel is 50 m long, horizontal, and frictionless, with rectangular cross sections 1 m wide. The initial water depth condition along the channel is

$$y(x) = \begin{cases} 1 \text{ m}, & 0 \text{ m} \leqslant x \leqslant 25 \text{ m} \\ 10^{-30} \text{ m}, & 25 \text{ m} < x \leqslant 50 \text{ m} \end{cases} \tag{20}$$

The exact solution of this problem can be found in Toro (2001). In the computation the channel is represented by 500 cells (Δx=0.1 m) and N_{CFL} is set equal to 0.01. Adopting a spatial step size equal to 0.1 m, no significant difference in the solutions appears by using different N_{CFL} numbers until the value of 0.9.

To treat the dry bed condition the only check that must be added to the numerical scheme is to assign a zero value to the momentum flux if the water depth on both sides of the cell interface are less than a very small depth y_{min}, set in the present case equal to 10^{-30} m (Sanders 2001).

In Figs. 7(a and b) the profiles of the computed and of the exact solutions of water level surface and velocity are reported at two different times: t=2 and 3 s. Fig. 7(a) shows the water level surface is computed well by the model with no appreciable error. The numerical solution is stable, monotone, and accurate, although it is slightly diffusive near the discontinuity at the upstream edge of the wave. However, Fig. 7(b) reveals that the numerical solution of the velocity profile is underpredicted near the wave front edge in a very limited region. This inaccuracy is a very common feature of numerical schemes, such as the Roe-type Riemann solver with the MUSCL approach proposed by Sanders

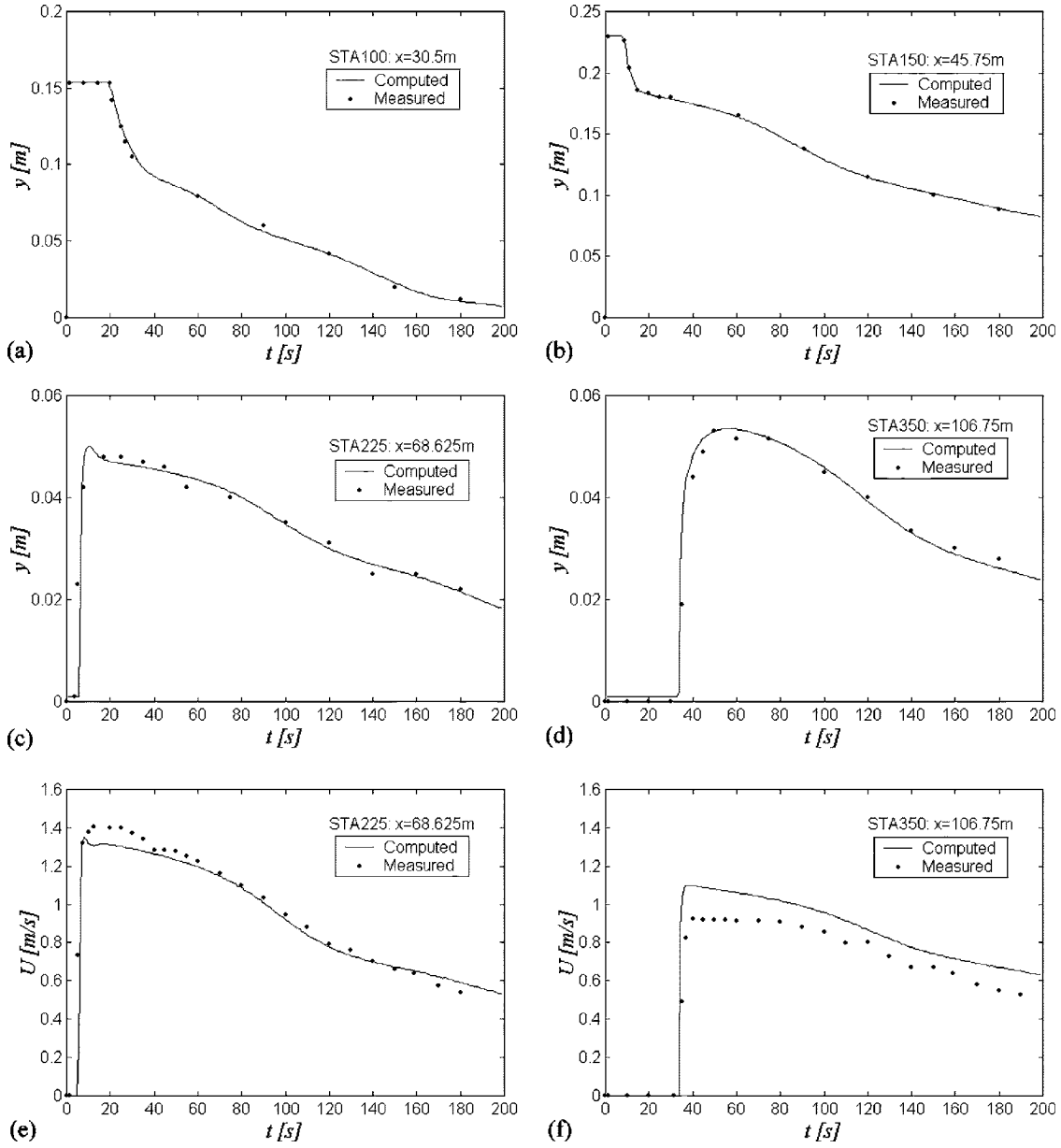

Fig. 8. Comparisons between numerical results and experimental data of WES partial dam-break problem: (a)–(d) water surface profiles; (e)–(f) velocity profiles

(2001), and the upwind conservative scheme with a weighted average surface gradient approach proposed by Ying et al. (2004). An underprediction of the water surface profile near the leading front edge is also shown by the numerical scheme proposed by Capart et al. (2003).

Test 7: Idealized Dam-Break Problem with Wet Bed

This test is the well-known dam-break problem with a wet bed and is presented to examine the model capability to capture shock and to deal with discontinuities in the numerical solution.

The channel geometry and the boundary conditions are the same of those used by Toro and Siviglia (2003). The channel is 50 m long, and 1 m wide, with rectangular cross sections and with horizontal and frictionless bed. The initial water depth condition along the channel is

$$y(x) = \begin{cases} 1 \text{ m}, & 0 \text{ m} \leqslant x \leqslant 25 \text{ m} \\ 0.5 \text{ m}, & 25 \text{ m} < x \leqslant 50 \text{ m} \end{cases} \tag{21}$$

The exact solution of this problem is reported in Toro (2001). The computational conditions are the same as those in Test 6.

In Figs. 7(c and d) water level surface and velocity profiles of the computed and of the exact solutions are displayed, respectively, at two different times: $t=2$ and 7 s. It can be seen that the numerical scheme has no diffusive behavior near the discontinuities, no oscillatory solution near large gradients (shock, contact, and in the vicinity of the rarefaction tail), and the shock position has a very small error.

The scheme is then tested by applying it to the same channel geometry but with a different initial flow depth condition defined as follows:

$$y(x) = \begin{cases} 1 \text{ m}, & 0 \text{ m} \leq x \leq 25 \text{ m} \\ 0.1 \text{ m}, & 25 \text{ m} < x \leq 50 \text{ m} \end{cases} \quad (22)$$

In this case, for a downstream water depth of 0.1 m, the flow depth for the positive wave from upstream is lower than the flow depth around which the negative wave profile swivels. Since the point of swivel is always the same, the negative wave from downstream controls the discharge value (Graf 1998) and the type of flow from the upstream positive wave is supercritical.

In Figs. 7(e and f) water level surface and velocity profiles of the computed and of the exact solutions are displayed at the same two times: $t=2$ and 7 s. Results again show a good performance of the present model.

As already discussed in Test 6, the idealized dam-break problem with wet bed also shows that no difference in the solutions appears by using different N_{CFL} values ranging between 0.005 and 0.9, and by adopting a spatial step size equal to 0.1 m.

Test 8: Partial Dam-Break Problem

The scheme is now tested with a partial dam break problem by comparing the numerical results with the data collected from laboratory experiments at the Waterways Experiment Station (WES) of the U.S. Army Corps of Engineers (WES 1960). The experiments were carried out in a rectangular flume 122 m long, 1.22 m wide, with a bottom slope of 0.005 and a Manning coefficient equal to 0.009 $\text{s}/\text{m}^{1/3}$. A removable dam 0.305 m high was located at the flume midpoint. Initially, the water depth upstream of the dam was as high as the top of the dam, while the bed was dry downstream. At $t=0$ s, a breach 0.183 m high and 0.732 m wide was suddenly generated in the middle part of the dam. This is a rigorous test due to the contraction in the channel width at the dam.

In the computation the flume is represented by 200 cells ($\Delta x=0.61$ m), N_{CFL} is set equal to 0.1, and no boundary condition is needed at either the upstream or at the downstream end of the flume. Note that the model solution is not dependent on the N_{CFL} number. The dry bed condition is treated in the same manner as in the dry bed dam-break problem, i.e., setting y_{min} equal to 0.001 m. This relatively larger value is due to the abrupt changes in the flume bottom (Ying et al. 2004).

Figs. 8(a–d) show a comparison between computed and measured water depth versus time at four different locations along the flume. The measurement stations reported here are: STA100 ($x=30.5$ m measured from the upstream boundary), STA150 ($x=45.75$ m), STA225 ($x=68.625$ m), and STA350 ($x=106.75$ m). The agreement between the numerical prediction and the experimental results is excellent.

In Figs. 8(e and f) the predicted velocity hydrographs at the two downstream stations (STA225 and STA350) compare well with the measured data, although Fig. 8(f) does illustrate that the numerical results slightly overpredict the experimental measurements. This was also shown by both Sanders (2001) and Ying et al. (2004).

The numerical scheme is able to accurately predict the wave advancing front in the flume and the assumption of a very small water depth y_{min} (equal to 0.001 m) for the flow modeling over the dry bed does not affect the accuracy of the computed results.

Test 9: Partial Dam-Break Problem with Overtopping Flow

This numerical problem proposed by Ying et al. (2004) was simulated to investigate the ability of the scheme to deal with complex open channel flow.

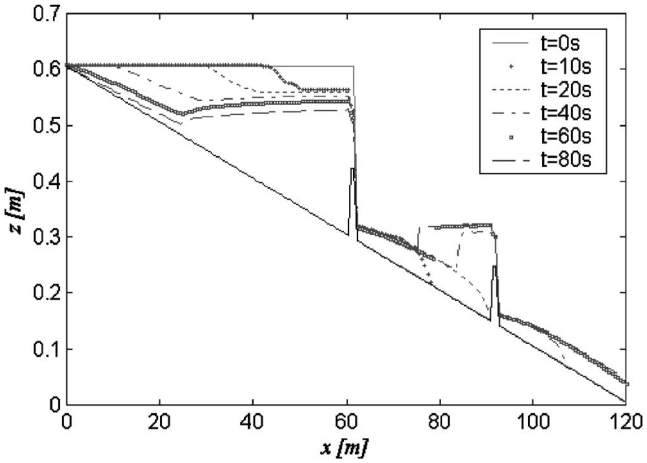

Fig. 9. Numerical solutions of Ying et al. (2004): partial dam-break problem with overtopping flow

The channel geometry is the same as the WES partial dam-break problem to which a 0.1 m high weir located 30.5 m downstream of the breached dam is added. The computational conditions are the same as in the previous test.

In Fig. 9 water level profiles are plotted at five different times ($t=10$, 20, 40, 60, and 80 s). Unfortunately no comparison with analytical solutions or experimental data are available, but the present results show the scheme is able to model a partial dam-break problem with overtopping flow and hydraulic jump (also see results reported by Ying et al. 2004).

Versilia River Case Study

Unsteady Flow in Versilia River

Finally, the numerical scheme was applied to simulate the propagation of a flood wave in the Versilia River, Italy. The numerical results are compared with data collected at a water level gauge located 6,580 m downstream of the inflow condition. The river geometry and the computational conditions are the same as those in Test 5. Note that the chosen N_{CFL} value is set equal to 0.85 and it corresponds to the maximum allowed by numerical stability. N_{CFL} values lower than 0.85 do not affect the solution. Moreover the Manning coefficient is varied from 0.031 to 0.029 $\text{s}/\text{m}^{1/3}$ in order to fit the gauged data. The measured discharge hydrograph imposed at the upstream boundary is shown in Fig. 10(a). The hydrograph begins on May 5, 2004 at 4:00 p.m. and finishes on May 7, 2004 at 1:00 a.m., lasting for 35 h. The discharge values range between 22 and 137 m^3/s.

Fig. 10(b) reveals that the computed water level hydrograph reproduces the gauged data quite well. Numerical results appear to slightly overestimate the water depth at the beginning of the hydrograph due to the uncertainty of initial conditions obtained from a steady flow simulation with the initial flow discharge.

The present results demonstrate the model's capability to reproduce correctly unsteady flow that contains several transcritical flows in a natural channel with irregular cross sections, and strongly nonuniform grids.

Conclusions

A numerical scheme able to deal with shocks and various types of flow transition in nonrectangular and nonprismatic channels, that

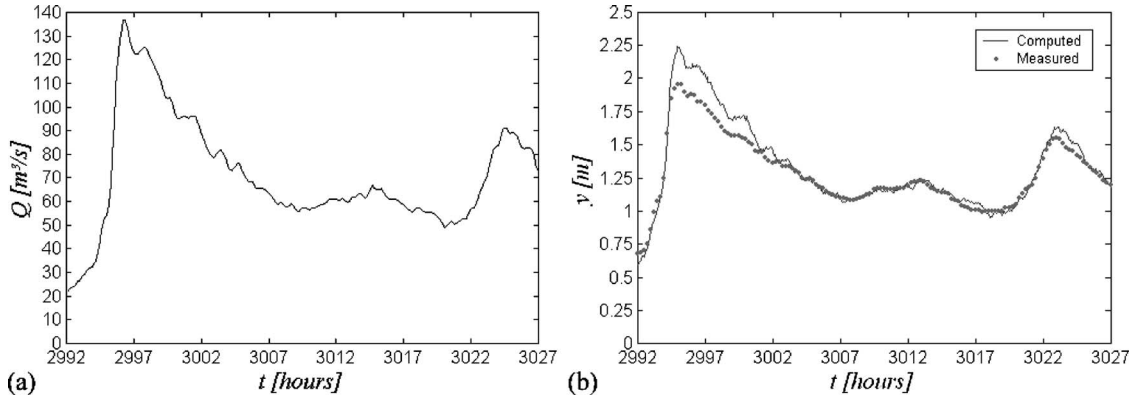

Fig. 10. Unsteady flow in Versilia River: (a) gauged discharge hydrograph imposed at upstream boundary; (b) computed and gauged water level hydrograph about 6.6 km downstream of upstream boundary

guarantees mass conservation and the balance of forces and momentum flux in the momentum equation, has been developed.

Due to the irregular channel geometry, particular attention is paid to the treatment of source terms by employing the recent findings of Schippa and Valiani (2002) and Capart et al. (2003). Following these formulations the channel bed slope term is not explicitly included in the Saint-Venant equations, thus preventing numerically generated flow and nonconservative solutions.

The Saint-Venant equations are written in a conservative form and are solved employing an explicit two step finite-volume scheme. The governing equation system is solved for the wetted cross-section area and flow discharge in each cell. The intercell fluxes are directly evaluated by means of the hydraulic variables previously assigned to each cell face. The assignment of the unknown variables along the cell faces is based on a Froude criterion of the upstream and downstream average cell flow across the face.

The main characteristic of the present method is the representation of the flow quantities in a conservative form within each cell independently from the spatial computational grid. Thus the method developed is particularly suitable for natural river flow modeling where wetted cross-sectional areas due to the irregularities of channel topography can be very different at the vertical interfaces of each cell.

The scheme has been successfully applied to various steady and unsteady benchmark problems, including subcritical, supercritical, and transcritical flows such as: water at rest in a channel with irregular topography; a hydraulic jump in a uniform and divergent rectangular horizontal channel; flow over a bump in a rectangular horizontal channel; an idealized dam-break problem in a rectangular horizontal channel with dry and wet bed; and finally a partial dam-break problem with a hydraulic jump and overtopping flow in a channel with irregular geometry.

These benchmark tests have shown that the scheme produces accurate solutions that agree well with corresponding analytical solutions or experimental data.

The present scheme was also applied to model flood propagation in the upper reach of the Versilia River, Tuscany, Italy. The 8 km channel reach was discretized by 169 cross sections with a strong nonuniform grid with cell size ranging from 2 to 264 m without any interpolation of topographic survey data. The numerical results were sufficiently robust to accurately reproduce the gauged stage hydrograph located about 6.6 km downstream of the upstream boundary.

The results presented for a range of test cases clearly demonstrate that the scheme is simple, stable, accurate, monotone, nonoscillating, and particularly robust, thus making the model suitable for addressing many problems in river management and civil protection.

Acknowledgments

The writers wish to acknowledge Professor Luigi Montefusco for his help and his valuable comments and suggestions. The writers also acknowledge Giulio Bechi for his comments and help with the numerical simulations. This work has received financial support from the IMONT National Mountain Institute for the research "Modellistica Numerica Applicata alla Propagazione delle Piene nei Corsi d'acqua Montani."

Appendix. Source Term Reformulation

Considering an arbitrary cell defined by the channel reach included between two vertical cross sections $S_{j-1/2}$ and $S_{j-1/2}$ located at $x_{j-1/2}$ and $x_{j+1/2}$, respectively, and assuming a linear variation of all the variables it appears that

$$S(\xi) = S_{j-1/2} + \frac{S_{j+1/2} - S_{j-1/2}}{x_{j+1/2} - x_{j-1/2}}(x - x_{j-1/2}) = S_{j-1/2} + \frac{S_{j+1/2} - S_{j-1/2}}{\Delta x_j}\xi = S_{j-1/2} + \alpha_1 \xi \tag{23a}$$

$$h(\xi) = h_{j-1/2} + \frac{h_{j+1/2} - h_{j-1/2}}{x_{j+1/2} - x_{j-1/2}}(x - x_{j-1/2}) = h_{j-1/2} + \frac{h_{j+1/2} - h_{j-1/2}}{\Delta x_j}\xi = h_{j-1/2} + \alpha_2 \xi \tag{23b}$$

$$z_g(\xi) = z_{gj-1/2} + \frac{z_{gj+1/2} - z_{gj-1/2}}{x_{gj+1/2} - x_{gj-1/2}}(x - x_{j-1/2}) = z_{gj-1/2} + \frac{z_{gj+1/2} - z_{gj-1/2}}{\Delta x_j}\xi = z_{gj-1/2} + \alpha_3 \xi \tag{23c}$$

where $\xi = x - x_{j-1/2}$; $\Delta x_j = x_{j+1} - x_j$; $\alpha_1 = (S_{j+1/2} - S_{j-1/2})/\Delta x_j$; $\alpha_2 = (h_{j+1/2} - h_{j-1/2})/\Delta x_j$; and $\alpha_3 = (z_{gj+1/2} - z_{gj-1/2})/\Delta x_j$.

Under the assumption that the two vertical cross sections are separated by an infinitesimal distance dx, following Schippa and Valiani (2002) and Capart et al. (2003), it is reasonable to assume that the hydrostatic pressure force in the direction of the main stream due to the reaction of the channel walls in the case of variations in shape along this direction is expressed as

$$\gamma \left.\frac{\partial I_1}{\partial x}\right|_{h_m} dx \tag{24}$$

where h_m=average elevation of the water surface within the cell.

Integrating Eq. (24) between the cross sections $j-1/2$ and $j+1/2$, we obtain

$$\zeta = \int_{x_{j-1/2}}^{x_{j+1/2}} \left.\frac{\partial I_1}{\partial x}\right|_{h_{mj}} dx = \int_0^{\Delta x_j} \left.\frac{\partial I_1}{\partial x}\right|_{h_{mj}} d\xi \tag{25}$$

being $I_1=S\cdot(h_m-z_g)$ it is $\partial I_1/\partial x=\partial S/\partial x\cdot(h_m-z_g)-S\partial z_g/\partial x$, and thus Eq. (25) becomes

$$\zeta = \int_0^{\Delta x_j} \left(\frac{\partial S}{\partial x}\cdot(h_{mj}-z_g) - S\cdot\frac{\partial z_g}{\partial x}\right) d\xi \tag{26}$$

Observing that $\partial S/\partial x=(S_{j+1/2}-S_{j-1/2})/\Delta x_j=\alpha_1$, $\partial z_g/\partial x=(z_{gj+1/2}-z_{gj-1/2})/\Delta x_j=\alpha_3$; it is seen that

$$\begin{aligned}\zeta &= \int_0^{\Delta x_j} \{\alpha_1[h_{mj}-(z_{gj-1/2}+\alpha_3\xi)]-\alpha_3(S_{j-1/2}+\alpha_1\xi)\}d\xi \\ &= \alpha_1\Delta x_j\left[h_{mj}-\left(z_{gj-1/2}+\alpha_3\frac{\Delta x_j}{2}\right)\right]-\alpha_3\Delta x_j\left(S_{j-1/2}+\alpha_1\frac{\Delta x_j}{2}\right)\end{aligned} \tag{27}$$

and finally

$$\begin{aligned}\zeta &= \tfrac{1}{2}(S_{j+1/2}-S_{j-1/2})[2h_{mj}-(z_{gj+1/2}+z_{gj-1/2})]-\tfrac{1}{2}(z_{gj+1/2}-z_{gj-1/2}) \\ &\times(S_{j+1/2}+S_{j-1/2}) = [S_{j+1/2}(h_{mj}-z_{gj+1/2})-S_{j-1/2}(h_{mj}-z_{gj-1/2})]\end{aligned} \tag{28}$$

Notation

The following symbols are used in this paper:

$B_{j\pm1/2}$ = wetted perimeter at $j\pm1/2$th intercell;
b = channel width at water surface;
C = dimensionless Chézy coefficient;
dx = negligible distance between two vertical cross sections;
$\mathbf{F}$ = vectors of conserved fluxes;
F_j = Froude number of average flow of jth cell;
$\bar{F}_{j+1/2}=\int_{S_{j+1/2}}(p+\rho v^2)\bar{i}dS$ = momentum function at the $j+1/2$th intercell;
G = arbitrary variable;
G_j = average value of arbitrary variable within jth cell;
g = gravitational acceleration;
h = water surface elevation;
h_{mj} = average elevation of water surface within jth cell;
I_1 = first moment of wetted cross section with respect to free surface;
J = energy loss gradient along y coordinate;
$\bar{k}$ = vertical unit coordinate;
N = number of grid points;
N_{CFL} = Courant–Friedrichs–Lewy number;
n = time step index;
$\bar{n}$ = unit vector outward normal to S;
p = pressure;
Q = liquid discharge;
Q_j = value of liquid discharge within jth cell;
q = liquid discharge per unit width;
$\mathbf{S}$ = vectors of source terms;
S = wetted control surface;
S_j = value of wetted cross-sectional area within jth cell;
$S_{j+1/2}$ = wetted cross section at $j+1/2$th interface;
S_l = wetted surface of control volume;
S_{pl} = water surface of control volume;
t = temporal coordinate;
$\mathbf{U}$ = vectors of conserved variables;
V = control volume;
$\bar{v}$ = local velocity averaged over turbulence;
x = spatial coordinate of x axis;
$x_{j+1/2}$ = locations of $j+1/2$th vertical cross section orthogonal to x axis;
y = water depth;
z_f = bottom elevation;
z_g = center mass elevation of wetted cross section;
α = Coriolis velocity distribution coefficient;
β = Boussinesq velocity distribution coefficient;
γ = unit weight;
Δt = time interval;
Δt^n = distance between temporal coordinates t^n and t^{n+1};
Δx = cell length;
Δx_j = distance between vertical cross sections $j-1/2$ and $j+1/2$;
ρ = density of water; and
$\bar{\tau}$ = shear stress (viscous+turbulent).

References

Alcrudo, F., Garcia-Navarro, P., and Savirón, J. M. (1992). "Flux difference splitting for 1D open channel flow equations." *Int. J. Numer. Methods Fluids*, 14, 1009–1018.

Bermudez, A., and Vazquez, M. E. (1994). "Upwind methods for hyperbolic conservation laws with source terms." *Comput. Fluids*, 23(8), 1049–1071.

Burguete, J., and Garcia-Navarro, P. (2001). "Efficient construction of high-resolution TVD conservative schemes for equations with source terms: Application to shallow water flows." *Int. J. Numer. Methods Fluids*, 37, 209–248.

Capart, H., Eldho, T. I., Huang, S. Y., Young, D. L., and Zech, Y. (2003). "Treatment of natural geometry in finite volume river flow computations." *J. Hydraul. Eng.*, 129(5), 385–393.

Chow, V. T. (1959). *Open-channel hydraulics*, McGraw-Hill, New York.

Garcia-Navarro, P., Alcrudo, F., and Savirón, J. M. (1992). "1D open-channel flow simulation using TVD-McCormack scheme." *J. Hydraul. Eng.*, 118(10), 1359–1372.

Garcia-Navarro, P., and Vázquez-Cendón, M. E. (2000). "On numerical treatment of the source terms in the shallow water equations." *Comput. Fluids*, 29, 951–979.

Gharangik, A. M., and Chaudhry, M. H. (1991). "Numerical simulation of hydraulic jump." *J. Hydraul. Eng.*, 117(9), 1195–1211.

Goutal, N., and Maurel, F. (1997). *Proc., 2nd Workshop on Dambreak*

Simulation. Direction des Ètudes et Recherches. EDF Rep. No. HE-43/97/016/B, Lisbon, Portugal, Electricité de France, Départment Laboratoire National d'Hydraulique, Groupe Hydraulique Fluviale, Lyon.

Graf, W. (1998). *Fluvial hydraulics*, Wiley, Chichester, U.K.

Jin, M., and Fread, D. L. (1997). "Dynamic flood routing with explicit and implicit numerical solution schemes." *J. Hydraul. Eng.*, 123(3), 166–173.

Khalifa, A. M. (1980). "Theoretical and experimental study of the radial hydraulic jump." Ph.D. thesis, Univ. of Windsor, Windsor, Ont., Canada.

Mingham, C. G., and Causon, D. M. (1998). "High-resolution finite-volume method for shallow water flows." *J. Hydraul. Eng.*, 124(6), 605–614.

Molls, T., and Molls, F. (1998). "Space-time conservation method applied to Saint-Venant equations." *J. Hydraul. Eng.*, 124(5), 501–508.

Nujić, M. (1995). "Efficient implementation of non-oscillatory schemes for the computation of free-surface flows." *J. Hydraul. Res.*, 33(1), 101–111.

Sanders, B. F. (2001). "High-resolution and non-oscillatory solution of the Saint-Venant equations in non-rectangular and non-prismatic channels." *J. Hydraul. Res.*, 39(3), 321–330.

Savic, L. J., and Holly, F. M. (1993). "Dambreak flood waves computed by modified Godunov method." *J. Hydraul. Res.*, 31(2), 187–204.

Schippa, L., and Valiani, A. (2002). "Un metodo per la trattazione del termine sorgente per la propagazione in alvei naturali a geometria complessa." *Proc., 28th Convegno di Idraulica e Costruzioni idrauliche*, Bios, ed., Cosenza, Italy, 175–182 (in Italian).

Siviglia, A., Colombini, M., and Toro, E. F. (2002). "Soluzione numerica di correnti a superficie libera: Forma non-conservativa e ruolo dei termini sorgente." *Proc., 28th Convegno di Idraulica e Costruzioni idrauliche*, Bios, ed., Cosenza, Italy, 175–182 (in Italian).

Toro, E. F. (2001). *Shock-capturing methods for free-surface shallow flows*, Wiley, New York.

Toro, E. F., and Siviglia, A. (2003). "PRICE: Primitive centered schemes for hyperbolic systems." *Int. J. Numer. Methods Fluids*, 42, 1263–1291.

Tseng, M. H., Hsu, C. A., and Chu, C. R. (2001). "Channel routing in open-channel flows with surges." *J. Hydraul. Eng.*, 127(2), 115–122.

Valiani, A., Califfi, V., and Bernini, A. (2004). "Schemi CWENO per l'integrazione numerica delle equazioni alle acque basse." *Proc., 29th Convegno di Idraulica e Costruzioni idrauliche*, Bios, ed., Cosenza, Italy, 915–921 (in Italian).

Vázquez-Cendón, M. E. (1999). "Improved treatment of source terms in upwind schemes for the shallow water equations in channel with irregular geometry." *J. Comput. Phys.*, 148, 497–526.

Wang, J. S., Ni, H. G., and He, Y. S. (2000). "Finite-difference TVD scheme for computation of dam-break problems." *J. Hydraul. Eng.*, 126(4), 253–262.

Waterways Experiment Station (WES). (1960). "Floods resulting from suddenly breached dams." *Miscellaneous Paper No. 2-374, Rep. No. 1*: *Conditions of Minimum Resistance*, U.S. Army Corps of Engineers, Vicksburg, Miss.

Yang, J. Y., Hsu, C. A., and Chang, S. H. (1993). "Computations of free surface flows. Part 1: One-dimensional dam-break flow." *J. Hydraul. Res.*, 31(1), 19–34.

Ying, X., Khan, A. A., and Wang, S. S. Y. (2004). "Upwind conservative scheme for the Saint-Venant equations." *J. Hydraul. Eng.*, 130(10), 977–987.

Younus, M., and Chaudhry, M. H. (1994). "A depth-averaged k-$\in$ turbulence model for the computation of free-surface flow." *J. Hydraul. Res.*, 32(3), 415–444.

Zhou, J. G., Causon, D. M., Mingham, C. G., and Ingram, D. M. (2001). "The surface gradient method for the treatment of surface terms in the shallow-water equations." *J. Comput. Phys.*, 168, 1–25.